

Highlights

A Learned SVD approach for Inverse Problem Regularization in Diffuse Optical Tomography

Alessandro Benfenati, Giuseppe Bisazza, Paola Causin

- Inverse problems arising in Diffuse Optical Tomography are severely ill-conditioned
- Traditional approaches rely on regularization functions with fine tuning of parameters
- We explore deep learning techniques in a fully data-driven approach
- The approach is the deep learning equivalent of the SVD of a nonlinear functional
- The solution is robust even in presence of high levels of noise

A Learned SVD approach for Inverse Problem Regularization in Diffuse Optical Tomography

Alessandro Benfenati^{a,1,*}, Giuseppe Bisazza^c, Paola Causin^{c,1}

^a*Department of Environmental and Science Policy, Via Celoria 2, Milan, 20133, Italy,*

^b*GNCS, INDAM,*

^c*Department of Mathematics, Via Saldini 50, Milan, 20133, Italy,*

Abstract

Diffuse Optical Tomography (DOT) is an emerging technology in medical imaging which employs near-infra-red light to estimate the distribution of optical coefficients in biological tissues for diagnostic purposes. The DOT approach involves the solution of a severely ill-posed inverse problem, for which regularization techniques are mandatory in order to achieve reasonable results. Traditionally, regularization techniques put a variance prior on the desired solution/gradient via regularization parameters, whose choice requires a fine tuning. In this work we explore deep learning techniques in a fully data-driven approach, able of reconstructing the generating signal (absorption coefficient) in an automated way. We base our approach on the so-called learned Singular Value Decomposition, which has been proposed for general inverse problems, and we tailor it to the DOT application. We test our approach on a 2D synthetic dataset, with increasing levels of noise on the measure.

Keywords: Diffuse Optical Tomography, Diffusion Equation, Inverse Problems, SVD, Deep Learning

1. Introduction

Diffuse Optical Tomography (DOT) is an emerging non-invasive and non-ionizing innovative approach for medical imaging. DOT employs near-infra-red light to estimate the spatial distribution of absorption and scattering coefficients within biological tissues. This information can be correlated to pathological conditions and used for diagnostic purposes [1]. A technical apparatus for DOT diagnostic consists in an arrays of N_s pointwise light sources emitting light on defined wavelengths into the tissue. The light exiting from the tissue is measured by detectors; for ease of presentation, we suppose to dispose of N_d detectors physically located on the tissue surface. We observe that in many practical implementations, a CCD camera collects the light and the pixels of the generated image are mapped on points of the tissue surface. This, however, does not impact on the following discussion. In this paper we suppose to work with a single light wavelength and in this setting we only approximate the absorption coefficient [2]. The reconstruction of the generating distribution of the absorption coefficient in the tissue is obtained via the solution of an inverse problem. Here we directly consider a finite dimensional formulation, so that we seek the vector $\boldsymbol{\mu}_a^* \in \mathbb{R}^{N_c \times 1}$ which represents the absorption coefficient evaluated in N_c collocation points in the tissue volume discretized in voxels and is such that

$$\boldsymbol{\mu}_a^* = \underset{\boldsymbol{\mu}_a}{\operatorname{argmin}} \mathcal{F}(\boldsymbol{\mu}_a) = \underset{\boldsymbol{\mu}_a}{\operatorname{argmin}} \frac{1}{2} \|\mathbf{y} - \boldsymbol{\psi}(\boldsymbol{\mu}_a)\|_2^2. \quad (1)$$

In Eq. (1), $\boldsymbol{\psi} \in \mathbb{R}^{N_d \times N_s}$ is the vector of approximations of the light fluence in the N_d detectors due to each of the N_s sources obtained via the model of light propagation (forward problem) as

$$\boldsymbol{\psi} = \mathcal{A}(\boldsymbol{\mu}_a)|_d, \quad (2)$$

*Corresponding author: alessandro.benfenati@unimi.it

and $\mathbf{y} \in \mathbb{R}^{N_d \times N_s}$ is the (noisy) measure given by the multi-static data matrix

$$\mathbf{y} = \begin{bmatrix} \mathbf{u}^1(\mathbf{d}_1) & \mathbf{u}^2(\mathbf{d}_1) & \dots & \mathbf{u}^{N_s}(\mathbf{d}_1) \\ \mathbf{u}^1(\mathbf{d}_2) & \mathbf{u}^2(\mathbf{d}_2) & \dots & \mathbf{u}^{N_s}(\mathbf{d}_2) \\ \vdots & \vdots & \ddots & \vdots \\ \mathbf{u}^1(\mathbf{d}_{N_d}) & \mathbf{u}^2(\mathbf{d}_{N_d}) & \dots & \mathbf{u}^{N_s}(\mathbf{d}_{N_d}) \end{bmatrix}. \quad (3)$$

The mapping \mathcal{A} , which in general is nonlinear, derives from the differential operator chosen to model light propagation in the tissue. A typical linear example of the operator \mathcal{A} is obtained considering a diffusive-reactive differential model for light propagation and adopting the Rytov perturbative approximation, in which one sets $\boldsymbol{\mu}_a = \boldsymbol{\mu}_{a,0} + \boldsymbol{\delta}\boldsymbol{\mu}_a$, $\boldsymbol{\mu}_{a,0}$ being the vector of known background values of the absorption and $\boldsymbol{\delta}\boldsymbol{\mu}_a$ the vector of unknown perturbations (see [3] for a detailed derivation). In this context, $\mathcal{A} \equiv \mathbf{J}$ and

$$\boldsymbol{\psi} = (\mathbf{J} \boldsymbol{\delta}\boldsymbol{\mu}_a)|_d, \quad (4)$$

where \mathbf{J} is the so-called sensitivity matrix. This matrix is the discrete counterpart of the Fredholm integral whose kernel is the Green’s function associated with the differential operator of the forward problem [4]. A more accurate nonlinear formulation stems from the Lippman–Schwinger equation, which amounts to consider also higher order terms in the Rytov perturbative approach [5]. In any case, the resulting inverse problem is severely ill-conditioned and regularization techniques are mandatory in order to obtain a physically coherent solution [6, 2]. One is then led to consider the following regularized optimization problem

$$\boldsymbol{\mu}_a^{*,\mathcal{R}} = \underset{\boldsymbol{\mu}_a}{\operatorname{argmin}} \mathcal{F}(\boldsymbol{\mu}_a) + \alpha \mathcal{R}(\boldsymbol{\mu}_a), \quad (5)$$

where \mathcal{R} is a regularization function and the regularization parameter α balances its influence on the solution. Both the choice of the regularization function and the regularization parameter are crucial. A classical strategy is to choose \mathcal{R} as an ℓ_2 -norm, which sets a uniform variance prior on the desired solution (Tikhonov regularization or ridge regression), and to hand-pick α from a parametric analysis. Choosing \mathcal{R} as an ℓ_1 -norm promotes sparseness, the idea being that the DOT solution typically possesses only a (relatively) small number of non-zero components. In [7, 8] the Elastic-Net regularization term, involving a convex combination of ℓ_1 and ℓ_2 norms, was investigated for the 2D DOT problem under the Rytov approximation and yielded satisfactory results. In [9] this approach was validated for the 3D case. As an alternative, [7] presented another regularization strategy, based on Bregman iterations [10, 11], which consisted in using the Bregman Divergence. For each of these choices, a fine tuning of the regularization parameter was required. The parameter was observed to be strongly dependent on the specific setting: the geometry, the perturbation intensity and location, the level of noise were all involved factors. In this work, we aim to overcome the *a-priori* choice of the regularization and we pursue the idea to *learn* it via Neural Networks. This idea is not new in the field of regularization. For example, in [12] a general regularization term is learned even when only unsupervised data is available. In [13, 14] a Total Deep Variation functional was learned, while the NETT framework of [15] learned $\mathcal{R}(\cdot) = \|\mathcal{N}_e(\cdot)\|_q^q$, where \mathcal{N}_e was the encoder part of an encoder-decoder network. The parameter α was chosen a-priori and held fixed. At the best of our knowledge, very few literature works have explored the option of learning the regularization in DOT applications. In [16] a *Regularization by Denoising* (RED) approach was proposed, while [17] trained a Neural Network for inverting the Lippman–Schwinger equation, by firstly learning the pseudoinverse of the nonlinear mathematical operator modelling the DOT physics and then applying an encoder-autoencoder network to denoise. We refer to [18] for a review of other related techniques. Here we investigate and adapt the general strategy presented in [19], the so-called Learned SVD. This approach consists in mapping the measured data into a feature space (the “singular values”) and then use such hidden features, upon a learned regularization, to reconstruct the generating signal $\boldsymbol{\mu}_a$.

This paper is organized as follows. Section 2 presents the machine learning framework used to learn the problem regularization along with its connection with the SVD decomposition and the Tikhonov reg-

ularization; Section 3 presents the net implementation and the experimental results; Section 4 draws the conclusions.

2. Deep Learning Regularization

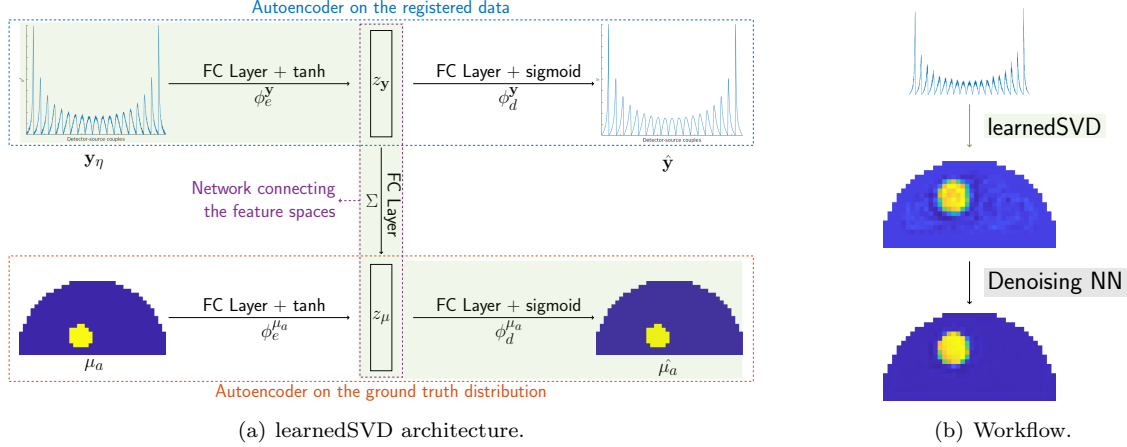


Figure 1: Left: LearnedSVD strategy for DOT reconstruction problem. The upper part of the scheme represents dAE: it receives as an input noisy data \mathbf{y}^η and it outputs a denoised version $\hat{\mathbf{y}}$. The bottom part represents the sAE: it reconstructs the noise-free ground truth. The operator Σ is learned in order to connect the two feature representations. The end-to-end workflow is enlightened in green and defines the mapping $\phi_d^{\mathbf{y}} \circ \Sigma \circ \phi_e^{\mathbf{y}}$. Right: the learnedSVD is applied to the data, then a denoising network [17] is used for cleaning the achieved result. Abbreviations: FC = Fully Connected layer, tanh = hyperbolic tangent activation function, sigmoid = sigmoid activation function.

We follow the L-SVD strategy of [19], named after the classical Singular Value Decomposition. As a matter of fact, when the operator \mathcal{A} is linear, as is the case of the Rytov approach for which $\mathcal{A} \equiv \mathbf{J}$, one may write $\mathbf{J} = \mathbf{U}\mathbf{S}\mathbf{V}^\top$, where \mathbf{S} is a diagonal matrix containing the singular values and express the solution as $\delta\boldsymbol{\mu}_a = \mathbf{V}\mathbf{S}^{-1}\mathbf{U}^\top \mathbf{y}$. The idea, which can be applied as well to nonlinear operators, is to write $\mathcal{A} = \mathcal{U} \circ \Sigma \circ \mathcal{V}$ and learn the decomposition via autoencoder (AE) architectures. To do this, similarly to [19], we consider two AEs: the first, called data-AE, acts on the noisy measure and is defined by

$$\mathbf{z}_y = \phi_e^y(\mathbf{y}), \quad \hat{\mathbf{y}} = \phi_d^y(\mathbf{z}_y), \quad (6)$$

where \mathbf{z}_y is the encoded feature (latent representation) of the noisy data \mathbf{y} and $\hat{\mathbf{y}}$ the decoded version. In the SVD framework, ϕ_e^y and ϕ_d^y can be seen as the correlative of \mathbf{U} and \mathbf{U}^\top for the linear case, respectively. This encoder-decoder has also a denoising behaviour by construction: the input data is noisy, and the AE is trained in order to provide a noise-free reconstruction. The second AE, called signal-AE (sAE), acts on the generating signal and is defined by

$$\mathbf{z}_\mu = \phi_e^\mu(\boldsymbol{\mu}_a), \quad \hat{\boldsymbol{\mu}}_a = \phi_d^\mu(\mathbf{z}_\mu) \quad (7)$$

where \mathbf{z}_μ is the encoded feature (latent representation) of the generating signal $\boldsymbol{\mu}_a$ and $\hat{\boldsymbol{\mu}}_a$ the decoded version. Within the SVD framework, the decoder ϕ_d^μ can be considered as the counterpart of \mathbf{V} . The two latent feature representations \mathbf{z}_y and \mathbf{z}_μ are related by the operator Σ , such that $\mathbf{z}_\mu = \Sigma(\mathbf{z}_y)$, which plays the scaling role of the singular values in \mathbf{S} in the classical SVD approach. The strategy consists thus in:

- i) Encoding the data \mathbf{y} in the latent space via the decoder ϕ_d^y : in the linear case, this corresponds to perform $\mathbf{U}^\top \mathbf{y}$.
- ii) Connecting the latent variables \mathbf{z}_y and \mathbf{z}_μ via the operator Σ : this mimics the computation $\mathbf{S}^{-1}\mathbf{U}^\top \mathbf{y}^\eta$.

- iii) Decoding the latent variables \mathbf{z}_μ into the coefficient distribution via the decoder ϕ_e^μ : this corresponds to the final left multiplication by \mathbf{V} in the SVD.

See Figure 1(a) for a visual inspection of the learnedSVD approach in the DOT context. Notice that this approach is fully *data-driven*.

Remark. *Classical Tikhonov regularization and SVD approaches have several points in common. Indeed, consider (5) when the operator is linear and \mathcal{R} is $\frac{1}{2}\|\cdot\|_2^2$: the solution to the problem can be written as*

$$\widehat{\delta\boldsymbol{\mu}}_\alpha = \sum_i \frac{\sigma_i}{\sigma_i^2 + \alpha} \langle \mathbf{u}_i, \mathbf{y} \rangle \mathbf{v}_i = \sum_i f_\alpha(\sigma_i) \langle \mathbf{u}_i, \mathbf{y} \rangle \mathbf{v}_i$$

where \mathbf{v}_i and \mathbf{u}_i are the i -th right and left eigenvectors and σ_i is the i -th singular value, respectively. This approach consists in filtering the singular values via the function $f_\alpha(\sigma) = \frac{\sigma}{\sigma^2 + \alpha}$. The Learned SVD approach tries to generalise this technique, on the one hand learning a new operator Σ which plays the role of the filtering function f , on the other hand learning the encoder ϕ_e^μ and the decoder ϕ_d^μ which corresponds to the right and left eigenvectors, respectively.

3. Implementation and Numerical Results

In this section we assess the performance of the proposed approach both for the noise-free and for the noisy cases on a synthetic phantom.

Setting. We considered synthetic measures generated via the diffusive-reactive forward model (we refer to [9] for details). The phantom is a 2D semidisk with radius 5 cm, discretized in 588 square voxels with side 0.25 cm. We considered 19 light sources positioned 1 mm inside the straight boundary and 20 detectors uniformly distributed on the semicircular portion of the boundary. The background coefficient was set to $\mu_{a,0} = 0.01 D$. The scattering coefficient was set to $\mu'_s = 0.1 \text{ cm}^{-1}$, and the diffusion coefficient was computed accordingly. To train the network, we generated a set of 1500 samples, each with one or two circular perturbed regions with random radii and placed randomly inside the domain. The perturbed regions were chosen to have absorption coefficient equal to 3, 4 or 5-fold the background coefficient. When there were two perturbed regions, each region could have different absorption coefficient. The test dataset used to evaluate the performance of the network contained 150 samples. We considered noise-free data as well as noisy measures, obtained by adding white Gaussian noise to the data with variance 1%, 3% or 5%, respectively.

Implementation of the network. We considered both the encoders in the dAE and in sAE nets to be fully connected layers coupled with a tanh activation function and both the corresponding decoders to be composed of a fully connected layer plus a sigmoid function. We investigated several options for the structure of the operator Σ . Preliminary tests showed that the best architecture is formed by 7 layers, each one consisting in a fully connected layer plus a tanh activation function. The training of the NNs was performed via the Stochastic Gradient Descent method, with default settings. The training strategy for the Learned SVD was the following: the dAE and the sAE were trained separately, with learning rate of 0.1 and 0.01, respectively. Then, using the hidden representations of the two networks we created the dataset to train the Σ network, using a learning rate 0.1. The final Learned SVD network (cf. Figure 1(a), green shaded area) is hence created by connecting the layers of the encoder of dAE, of the network Σ and of the decoder of sAE. For each network, the loss function was chosen as the Euclidean distance between the ground truth and the reconstructed data. The number of epochs was 2000 for each training procedure. The Learned SVD net provided good results, but still noisy: in order to remove these artifacts, we trained a further Deep Neural Network, which acts as a denoiser. To do this, we use the architecture of [17]. An illustration of the entire workflow is provided in fig. 1(b). The numerical experiments were carried on a laptop PC with operating system Linux 19.04, endowed with an Intel(R) Core(TM) i5-8250U CPU (1.60GHz) and 16 GiB RAM memory. The NN architectures were implemented in MatLab R2020b.

Numerical results: qualitative and quantitative evaluation. Figure 2 presents the results obtained for different samples in the test set with varying levels of noise. The red circles depict the exact position

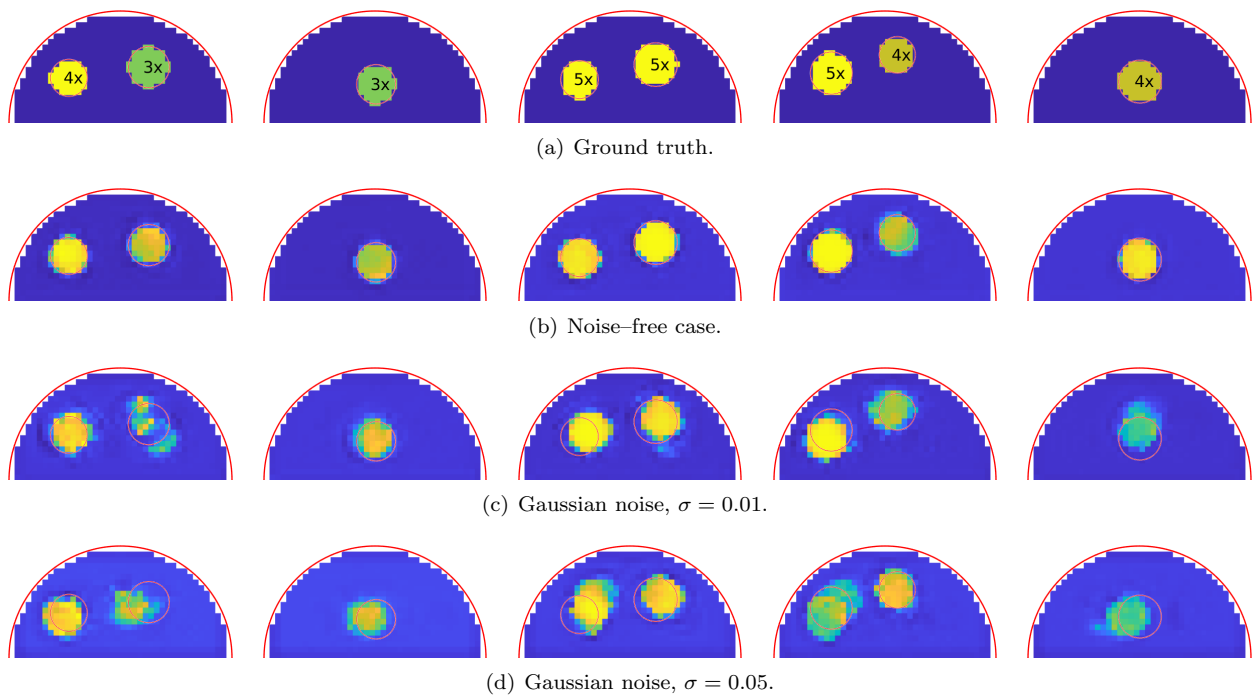


Figure 2: Reconstruction of the absorption coefficient distribution obtained with the Learned SVD approach. The red circles denote the exact position and extension of the perturbed regions (ground truth). First row refers to ground truth: each perturbed area presents its absorption coefficient, as a multiplier of the background one. The other rows depict the reconstructions in noise-free case (b), and white Gaussian noise with variance 1% (c) and 5% (d).

and radius of the perturbed region (ground-truth). In the noise-free case, the perturbed regions is almost perfectly recovered, both in location, shape and intensity. The other rows refer to the reconstruction obtained when Gaussian noise affects the measure. As one expects, the increasing noise level worsens the quality of the reconstruction but the gross location and shape of the perturbed region are correctly captured.

To quantitatively assess the performance of the proposed approach, we compute the average value of the absorption coefficient inside the reconstructed perturbed regions. We also assess the quality of the reconstructed extension via the True Positive Ratio (TPR) by checking how many pixels in the reconstruction are actually recognized as belonging to the true perturbed area. The results are summarized in Table 1, which presents the averages of these measurements obtained on the 150 samples of the test set.

Noise Level	$3\mu_{a,0}$ (GT: 9e-3)	$4\mu_{a,0}$ (GT: 1.2e-2)	$5\mu_{a,0}$ (GT: 1.5e-02)	TPR
0%	$9.06\text{e-}03 \pm 5.82\text{e-}04$	$1.22\text{e-}02 \pm 1.17\text{e-}03$	$1.43\text{e-}02 \pm 6.45\text{e-}04$	0.96
1%	$8.88\text{e-}03 \pm 8.67\text{e-}04$	$1.11\text{e-}02 \pm 1.79\text{e-}03$	$1.31\text{e-}02 \pm 1.30\text{e-}03$	0.81
3%	$8.75\text{e-}03 \pm 1.71\text{e-}03$	$1.06\text{e-}02 \pm 1.99\text{e-}03$	$1.21\text{e-}02 \pm 1.74\text{e-}03$	0.57
5%	$8.18\text{e-}03 \pm 1.39\text{e-}03$	$8.37\text{e-}03 \pm 1.76\text{e-}03$	$9.49\text{e-}03 \pm 2.33\text{e-}03$	0.58

Table 1: Intensity and TPR for the perturbed region for different noise levels. Values are averaged over 150 test samples. The nominal absorption coefficient values (GT, [cm^{-1}]) inside the perturbed regions are denoted in the head of the table.

We evince that increasing levels of noise worsen the TPR, while the reconstructed intensity of the absorption coefficient remains reliable. One should also notice that the reconstructed intensities approximate the nominal one by defect: this is not fully surprising, since SVD-based strategies are Tikhonov-like regularizations, which induce smoothing/blurring of the solution. On the other hand, there is still a notable difference with respect to the background value, and 58% of the extension of the perturbed regions is recovered on average, even for high noise levels.

4. Conclusions

In this work we have applied a Learned SVD approach to reconstruct the absorption coefficient distribution within a synthetic phantom imaged with the DOT technology. The inverse problem arising from such framework is severely ill-conditioned and demands a robust regularization. Here, we have addressed the inversion by a completely data-driven (fully learned) approach. As a matter of fact, the training of the network is done by using only the ground truths and the measure, without any information on the physical process and/or model beyond the data registration in DOT framework. This strategy has produced very accurate results in the noise-free case with average TPR of 97% and reasonable results for higher levels of noise. In this latter case the reconstructed coefficient is less accurate, but useful information about the presence and position of the perturbed regions is however conveyed. Future work will encompass the use of different models of noise and will be aimed at incorporating the information provided by the physical (forward) model into the structure of the network. A natural extension will regard data collected from 3D domains.

Acknowledgments. This work was supported by the PRECISION project, funded by University of Milan.

References

- [1] H. Jiang, Diffuse Optical Tomography: Principles and Applications, CRC Press, 2018.
- [2] C. Panagiotou, S. Somayajula, A. P. Gibson, M. Schweiger, R. M. Leahy, S. R. Arridge, Information theoretic regularization in diffuse optical tomography, J. Opt. Soc. Am. A 26 (5) (2009) 1277–1290. doi:10.1364/JOSAA.26.001277.
- [3] A. Ishimaru, Wave propagation and scattering in random media, Vol. 2, Academic Press New York, 1978.
- [4] D. Boas, D. Brooks, E. Miller, C. DiMarzio, M. Kilmer, R. Gaudette, Q. Zhang, Imaging the body with diffuse optical tomography, IEEE Signal Processing Magazine 18 (6) (2001) 57–75. doi:10.1109/79.962278.
- [5] A. Yodh, B. Chance, Spectroscopy and imaging with diffusing light, Physics Today 48 (3) (1995) 34–40. doi:doi:10.1063/1.881445.

- [6] G. Di Sciacca, L. Di Sieno, A. Farina, P. Lanka, E. Venturini, P. Panizza, A. Dalla Mora, A. Pifferi, P. Taroni, S. Arridge, Enhanced diffuse optical tomographic reconstruction using concurrent ultrasound information, *Philosophical Transactions of the Royal Society A* 379 (2204) (2021) 20200195.
- [7] A. Benfenati, P. Causin, M. Lupieri, G. Naldi, Regularization techniques for inverse problem in DOT applications 1476 (2020) 012007. doi:10.1088/1742-6596/1476/1/012007.
- [8] P. Causin, G. Naldi, R. Weishaepfl, Elastic net regularization in diffuse optical tomography applications, in: 2019 IEEE 16th International Symposium on Biomedical Imaging (ISBI 2019), 2019, pp. 1627–1630. doi:10.1109/ISBI.2019.8759476.
- [9] P. Causin, M. G. Lupieri, G. Naldi, R.-M. Weishaepfl, Mathematical and numerical challenges in optical screening of female breast, *International Journal for Numerical Methods in Biomedical Engineering* 36 (2) (2020) e3286. doi:https://doi.org/10.1002/cnm.3286.
- [10] A. Benfenati, V. Ruggiero, Inexact Bregman iteration with an application to Poisson data reconstruction, *Inverse Problems* 29 (6) (2013). doi:10.1088/0266-5611/29/6/065016.
- [11] X. Zhang, M. Burger, S. Osher, A unified primal-dual algorithm framework based on Bregman iteration, *Journal of Scientific Computing* 46 (1) (2011) 20–46. doi:10.1007/s10915-010-9408-8.
- [12] S. Lunz, O. Öktem, C.-B. Schönlieb, Adversarial regularizers in inverse problems, Vol. 2018-December, 2018, pp. 8507–8516, cited By 29.
- [13] E. Kobler, A. Effland, K. Kunisch, T. Pock, Total deep variation for linear inverse problems, in: *Proceedings of the IEEE/CVF Conference on Computer Vision and Pattern Recognition (CVPR)*, 2020.
- [14] E. Kobler, A. Effland, K. Kunisch, T. Pock, Total deep variation: A stable regularizer for inverse problems, *CoRR* abs/2006.08789 (2020). arXiv:2006.08789.
- [15] H. Li, J. Schwab, S. Antholzer, M. Haltmeier, NETT: solving inverse problems with deep neural networks 36 (6) (2020) 065005. doi:10.1088/1361-6420/ab6d57.
- [16] Z. Wu, Y. Sun, A. Matlock, J. Liu, L. Tian, U. S. Kamilov, SIMBA: Scalable inversion in optical tomography using deep denoising priors, *IEEE Journal of Selected Topics in Signal Processing* 14 (6) (2020) 1163–1175. doi:10.1109/JSTSP.2020.2999820.
- [17] J. Yoo, S. Sabir, D. Heo, K. Kim, A. Wahab, Y. Choi, S.-I. Lee, E. Chae, H. Kim, Y. Bae, Y.-W. Choi, S. Cho, J. Ye, Deep learning diffuse optical tomography, *IEEE Transactions on Medical Imaging* 39 (4) (2020) 877–887, cited By 18. doi:10.1109/TMI.2019.2936522.
- [18] L. Zhang, G. Zhang, Brief review on learning-based methods for optical tomography, *Journal of Innovative Optical Health Sciences* 12 (06) (2019) 1930011.
- [19] Y. E. Boink, C. Brune, Learned SVD: solving inverse problems via hybrid autoencoding, *CoRR* abs/1912.10840 (2019).